



# Influence of ferrite phase on electrical properties of the barium zirconium titanate based multiferroic composites

Adis S. Dzunuzovic<sup>1</sup> · M. M. Vijatovic Petrovic<sup>1</sup> · J. D. Bobic<sup>1</sup> · N. I. Ilic<sup>1</sup> · B. D. Stojanovic<sup>1</sup>

Received: 9 May 2020 / Accepted: 10 June 2021 / Published online: 16 June 2021

© The Author(s), under exclusive licence to Springer Science+Business Media, LLC, part of Springer Nature 2021

## Abstract

Multiferroic composites with general formula  $\text{Ba}(\text{Ti}_{0.95}\text{Zr}_{0.05})\text{O}_3 - \text{Ni}_{0.7}\text{Zn}_{0.3}\text{Fe}_2\text{O}_4$ ,  $\text{Ba}(\text{Ti}_{0.95}\text{Zr}_{0.05})\text{O}_3 - \text{CoFe}_2\text{O}_4$ ,  $\text{Ba}(\text{Ti}_{0.95}\text{Zr}_{0.05})\text{O}_3 - \text{Ni}_{0.7}\text{Cu}_{0.01}\text{Sm}_{0.05}\text{Zn}_{0.29}\text{Fe}_{1.95}\text{O}_4$ , (BTZr(95–5) – NZF, BTZr(95–5) – CF, BTZr(95–5) – NCuSmZF) were prepared by mixing chemically obtained different types of ferrites and BTZ(95–5) powders in the planetary mill for 24 h. The optimization of sintering process was performed and powders were pressed and sintered at 1300 °C for obtained composites samples. From the X-ray analysis for single phase and composites ceramics the formation of crystallized structure of ferrites and barium zirconium titanate can be noticed. SEM analyses indicated the formation of two types nanosized grains, polygonal ferromagnetic and rounded ferroelectric grains. The electrical properties of these materials were investigated using impedance spectroscopy and analysis of ferroelectric measurements. Impedance analysis of all investigated samples has shown different relaxation processes that originated from the grain and grain boundary contributions. The results of polarization vs. electric field measurements have shown the influence of magnetic phase type and its concentration on the ferroelectric properties of the composites. Due to high conductivity of ferrite phases and presence of interfacial polarization, the shapes of these curves differed from the conventional ferroelectric materials.

**Keywords** Composite materials · Ceramics · Grain boundaries · Impedance analysis

## 1 Introduction

During recent years studies of multiferroic materials and their application, functionality became very widespread. These materials was found to be useful in information storage, in the emerging field of spintronics, sensors, multistate memory devices, electrically tunable microwave devices such as filters, oscillators and phase shifters [1, 2]. For decades, researchers have been looking for a adequate way to couple magnetic and ferroelectric ordering in different materials. Recently, advances in materials fabrication made it possible to manufacture these kinds of materials in structures with smaller dimensions, such us thin films or complex composites including flexible structures. This is also very important in order to reduce the cost and improve the functionality of the system [3]. The term multiferroic is used for materials which simultaneously possess two or more primary ferroic (ferroelectric, ferromagnetic and ferroelastic) properties [4]. There are two

types of multiferroics: single phase multiferroics ( $\text{BiFeO}_3$ ,  $\text{BiMnO}_3$ ) and composites in many different combination of ferroelectric and ferromagnetic phases ( $(\text{NiZn})\text{Fe}_2\text{O}_4$ - $\text{BaTiO}_3$ ,  $\text{BaSrTiO}_3$ - $\text{Ni,ZnFe}_2\text{O}_4$ ,  $\text{Ni}(\text{Co, Mn})\text{Fe}_2\text{O}_4$ - $\text{BaTiO}_3$ ). The ferroelectric-ferromagnetic composites, as two-phase multiferroics, are greatly explored today and large number of publications about multiferroics were published so far [5–7]. Main advantage of ferroelectric-ferromagnetic composites in comparison with single phase multiferroics is much simpler synthesis method, since single phase multiferroics are very difficult to obtain under ambient conditions [8, 9]. However, it is also challenge to prepare composites materials with equilibrium ferroelectric and magnetic structures preserving both properties close to the room temperature. The influence of each phase in the composite multiferroics on the properties like resistivity, dielectric constant, ferroelectric, magnetic properties and others may be attributed to different relaxation process that occur in grains and grain boundaries of whole composite material but also the existence of different crystallographic phases should be taken into account in the same time.

In the previous studies, composites based on  $\text{BaTiO}_3$  (barium titanate, BT),  $\text{PbZr}_{0.52}\text{Ti}_{0.48}\text{O}_3$  (lead zirconium titanate, PZT) (as ferroelectric phases) and  $\text{NiZnFe}_2\text{O}_4$  (nickel zinc ferrite, NZF),  $\text{CoFe}_2\text{O}_4$  (cobalt ferrite, CF) (as ferromagnetic

✉ Adis S. Dzunuzovic  
a.dzunuz@hotmail.com

<sup>1</sup> Institute for Multidisciplinary Research, University of Belgrade, Belgrade, Serbia

phases) in different combination were investigated [6, 10–12]. BT possesses high permittivity, low dielectric losses and high tunability and was promoted as a material for the high speed and nonvolatile memory devices [13, 14]. It is well known that dielectric properties of barium titanate can be significantly modified by doping with  $\text{La}^{3+}$ ,  $\text{Mn}^{3+}$ ,  $\text{Zr}^{3+}$ ,  $\text{Hf}^{4+}$ ,  $\text{Nb}^{5+}$ , where the characteristic phase transition can be shifted to lower temperatures and doping can lead to the appearance of semiconductivity in the material [15, 16].  $\text{Ba}(\text{Ti}_y\text{Zr}_{1-y})\text{O}_3$  (BTZr) is derived from two perovskite lattices, barium titanate and barium zirconate. Zirconium substitution into the titanium lattices leads to enhancing the dielectric and piezoelectric properties [17, 18].  $\text{Ba}(\text{Ti}_{0.95}\text{Zr}_{0.05})\text{O}_3$  (BTZr(95–5)) has high dielectric constant, high piezoelectric coefficient, high tunability and low dielectric constant. BTZr ceramic, with the Zr content less than 10 mol%, show classical ferroelectric behavior and all three dielectric anomalies corresponding to cubic to tetragonal, tetragonal to orthorhombic and orthorhombic to rhombohedral phase transitions. These materials have proven to be very attractive and promising for dynamic random access memories and tunable microwave devices [19].

On the other side, NZF as a good soft magnetic and semi-hard CF with good electrostrictive properties, high value of magnetization and high chemical stability were investigated as a ferrite phase in the composites [20, 21]. Many reports are available in the literature for Cu-substituted NZF. M. Niyafar et al. reported that magnetization of  $\text{Ni}_{0.3}\text{Zn}_{0.7-x}\text{Cu}_x\text{Fe}_2\text{O}_4$  increase with Cu concentration up to  $x = 0.3$  [22]. Other authors have shown that Curie temperature increase for doped ferrites  $\text{Ni}_x\text{Zn}_{1-x}\text{Fe}_2\text{O}_4$  with Cu in comparison with pure  $\text{Ni}_x\text{Zn}_{1-x}\text{Fe}_2\text{O}_4$  ( $x = 0.3–0.7$ ), which can be attributed to the change of  $\text{Fe}^{3+}$  ions content on tetrahedral and octahedral sites due to presence of  $\text{Cu}^{2+}$  ions on octahedral sites [23, 24]. Also, addition of Cu in  $\text{NiCuZnFe}_2\text{O}_4$  can be used to improve densification as well as electromagnetic properties of the material [25]. The addition of samarium leads to increase the lattice parameter and decreases the mean grain size [26], permeability, magnetization and Curie temperature up to 0.02 at.% of Sm [27].

In the present paper, the preparation process and characterization of multiferroic composites based on ferroelectric phase BTZr(95–5) and different ferromagnetic phases: NZF, CF, NCuSmZF were presented. We were looking for a way to further improve the properties of existing composites. The structural, electric, ferroelectric properties of these composites materials were reported and explained in detail.

## 2 Material and methods

The raw materials used for the synthesis of magnetic phases, NZF, CF and NCuSmZF were  $\text{Fe}(\text{NO}_3)_3 \cdot 9\text{H}_2\text{O}$  (AlfaAesar, 98.0–101.0%),  $\text{Ni}(\text{NO}_3)_2 \cdot 6\text{H}_2\text{O}$  (AlfaAesar, 99.9985%),  $\text{Zn}(\text{NO}_3)_2 \cdot 6\text{H}_2\text{O}$  (Alfa Aesar, 99%),

$\text{Sm}(\text{NO}_3)_2 \cdot 6\text{H}_2\text{O}$  (Alfa Aesar, 99.9%),  $\text{Cu}(\text{NO}_3)_2 \cdot 3\text{H}_2\text{O}$  (Alfa Aesar, 99.9%),  $\text{C}_6\text{H}_8\text{O}_7 \cdot \text{H}_2\text{O}$  (CarloErba, 99.5–100.5%) and  $\text{NH}_4\text{OH}$  (LachNer, 25%). Metal nitrates and citric acid solution were mixed and after the process of self-propagation reaction and thermal treatment at 1000 °C the pure ferrite phase was obtained. Details of the auto-combustion method are reported earlier and can be found elsewhere [11, 28].

$\text{Ba}(\text{Ti}_{0.95}\text{Zr}_{0.05})\text{O}_3$  was synthesized by a modified auto-combustion synthesis. Starting reagents used for this synthesis were  $\text{Ti}(\text{OCH}(\text{CH}_3)_2)_4$  (TTIP) (AlfaAesar, 98.0–101.0%),  $\text{C}_6\text{H}_8\text{O}_7 \cdot \text{H}_2\text{O}$  (Carlo Erba, 99.5–100.5%),  $\text{Ba}(\text{NO}_3)_2$ ,  $\text{Zr}(\text{O}(\text{NO}_3)_2) \cdot 6\text{H}_2\text{O}$  (Alfa Aesar, 99.9%) and  $\text{NH}_4\text{OH}$  (Lach Ner, 25%). Obtained precursor powders were further calcined at 900 °C for 2 h. These powders were sintered at 1200 °C for 4 h in order to have pure BTZr ceramics for the comparison of its properties with multiferroics. The synthesis routes are schematically presented in Fig. 1.

Multiferroic composites BTZr(95–5) – NZF, BTZr(95–5) – CF, BTZr(95–5) – NCuSmZF were prepared by mixing chemically obtained powders of ferromagnetic and ferroelectric phases in a planetary ball mill for a 24 h in isopropyl alcohol as a milling medium. The mass ratio of ferroelectric and ferromagnetic phase was 80–20. The optimization of sintering process was performed and the powders were pressed at 195 MPa and sintered at 1300 °C for 4 h.

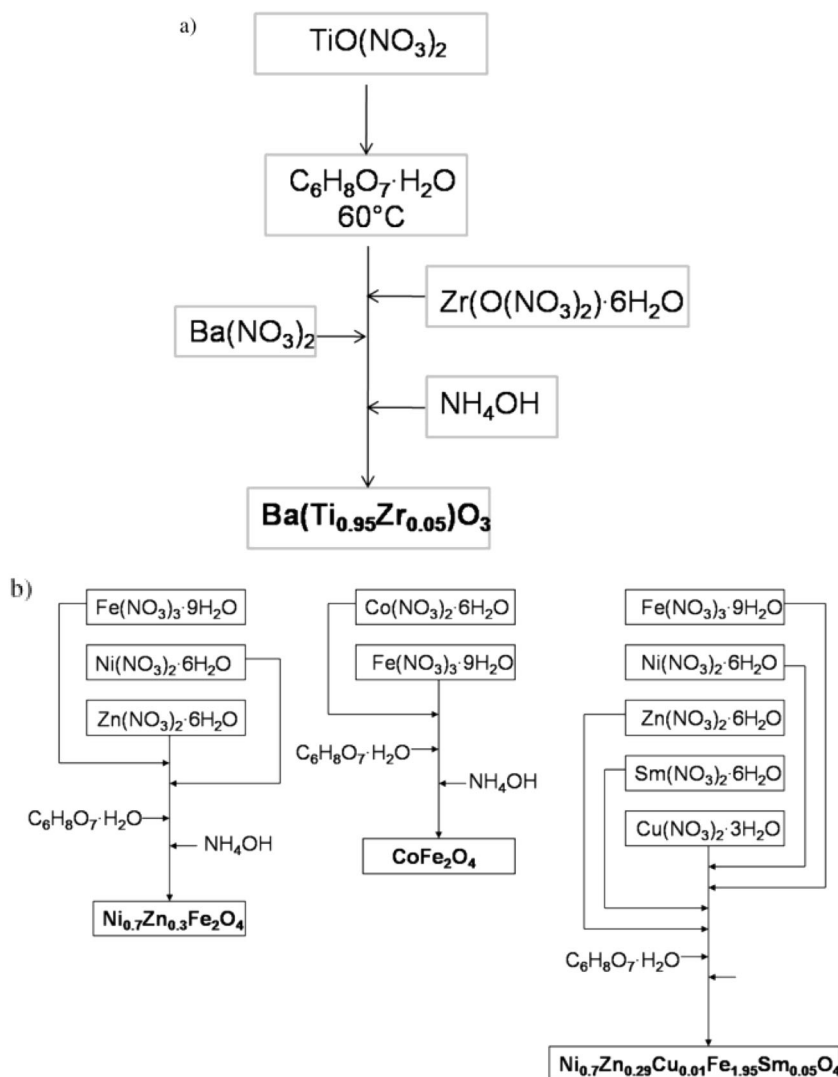
The phase and crystal structure of single phase materials as well as composites were investigated by X-ray diffractometer (Model Rigaku RINT 2000,  $\text{CuK}\alpha$  radiation). Scanning electron microscope (SEM) (Model TESCAN SM-300) was used for the microstructural characterization and the average grain size determination. The grain size was determined using an ImageJ program. Impedance spectroscopy of the sintered pellets was performed in the frequency range from 42 Hz to 1 MHz in the temperature range from 150 °C to 600 °C using an LCR meter (model 9593–01, HIOKI HITESTER). Collected data were analyzed using the commercial software package Z-view. Ferroelectric measurements were performed in the electrical field range from 10 to 38 kV/cm on the Precision Multiferroic Test System with High Voltage Interface (Radiant Technologies, Inc.). To study leakage current behavior of the ceramics, current density versus electric field was measured using the Precision Multiferroic Test System with High Voltage Interface (Radiant Technologies, Inc.).

## 3 Results and discussion

### 3.1 Structure and microstructure analysis

XRD patterns of sintered ferroelectric, ferromagnetic phase and also composites ceramics were presented in Fig. 2. The presence of the cubic spinel structure of NZF, NCuSmZF according to JCPDS card no. 10–0325 and CF according to

**Fig. 1** Scheme of (a) barium zirconium titanate and (b) ferrites preparation



JCPDS card no. 22–1086 was confirmed. The formation of perovskite tetragonal phase of BTZr(95–5) (according to JCPDS card no. 05–0626) was also observed. BaZrO<sub>3</sub> has a cubic structure at all temperatures. Also, additional Zr as a dopant in the BT structure led to formation of tetragonal structure of BTZr powder. X-ray measurements of obtained composites confirmed the presence of NZF, CF, NCuSmZF and BTZr(95–5) phases without the presence of any intermediate phases or impurities. Structural analysis of composites also showed the existence of the most prominent double peaks (evident peaks splitting) of the tetragonal phase of BTZr(95–5) at 32.5° and of the cubic ferrite phases that are located at 41.2° for NZF, 41.6° for CF and 42.2° for NCuSmZF. In order to obtain composites with only two phases and best possible densities the optimization of sintering process was performed. The most suitable sintering temperature for these composite materials was found to be 1300 °C (no secondary phases and interface reactions). Sintering time was also varied in order to obtain ceramics with optimal density. It was detected that

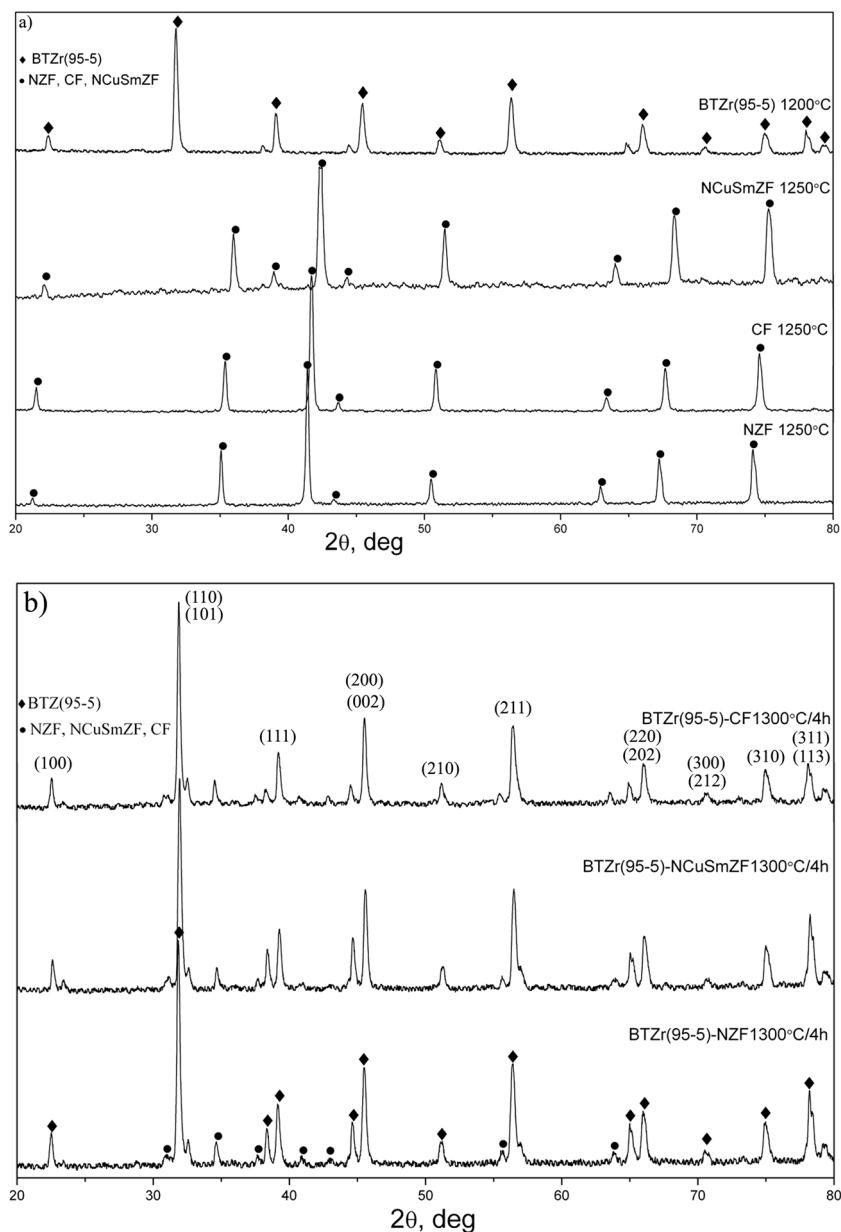
sintering below 4 h was short for proper grain growth especially for ferroelectric phase and longer sintering time lead to the interface reactions. Chosen sintering rate was 5 °C/min. Diagrams for composites ceramic samples presented the existence of characteristic splitting of diffraction peaks indicating strong tetragonality.

SEM images of obtained composites at the free surface are given in Fig. 3. The grains are below 1 μm with two different shapes: polygonal ferrite grains and more rounded grains of barium zirconium titanate. The average grain size for each composite was:

- ~ 0.71 μm for the sample BTZr(95–5)-NZF
- ~ 0.65 μm for the sample BTZr(95–5)-CF
- ~ 0.79 μm for the sample BTZr(95–5)-NCuSmZF

In these composites there is a mismatch between smaller and round barium zirconium titanate grains and bigger polygonal ferrite grains. Having this in mind as well as the difficulties in

**Fig. 2** XRD diffratograms of: (a) BTZr(95–5), NCuSmZF, CF, NZF, (b) BTZr(95–5)-CF, BTZr(95–5)-NCuSmZF, BTZr(95–5)-NZF ceramics



optimization of sintering process due to formation of secondary phases, relatively high composite density values have been obtained. Based on previous research, temperatures higher than 1350 °C can enable good density and reproducible electrical properties of the ferroelectric material. However, when ferroelectric material is bonded with magnetic phase in the multiferroics, secondary phase was formed on the interfaces. Therefore the most suitable sintering temperature for these kind of composites was found to be 1300 °C.

The density values were found to be 88.2, 92.6, 91.2% of the theoretical value for BTZr(95–5)-NZF, BTZr(95–5)-CF, BTZr(95–5)-NCuSmZF, respectively. The highest density values possesses BTZr(95–5)-CF which may be explained by the smallest average grain size in comparison with another two samples.

### 3.2 Impedance analysis

Variation of the imaginary part of impedance as a function of the real part of impedance gives the complex impedance spectrum- Nyquist plots [29, 30]. Impedance measurements were performed for all investigated ceramic composites in the temperature range from 150 °C to 600 °C for BTZr(95–5), from 150 °C to 250 °C for BTZr(95–5)-NZF, from 250 °C to 350 °C for BTZr(95–5)-CF and from 500 °C to 600 °C for BTZr(95–5)-NCuSmZF (Fig. 4.) and value of the grain, grain boundary and total electrical resistivity are presented in the Table 1. Due to high conductivity of the ferrite phase certain composites at some temperatures did not show semicircles that can be used in impedance analysis. Therefore, it was not possible to display measurements in a uniform temperature

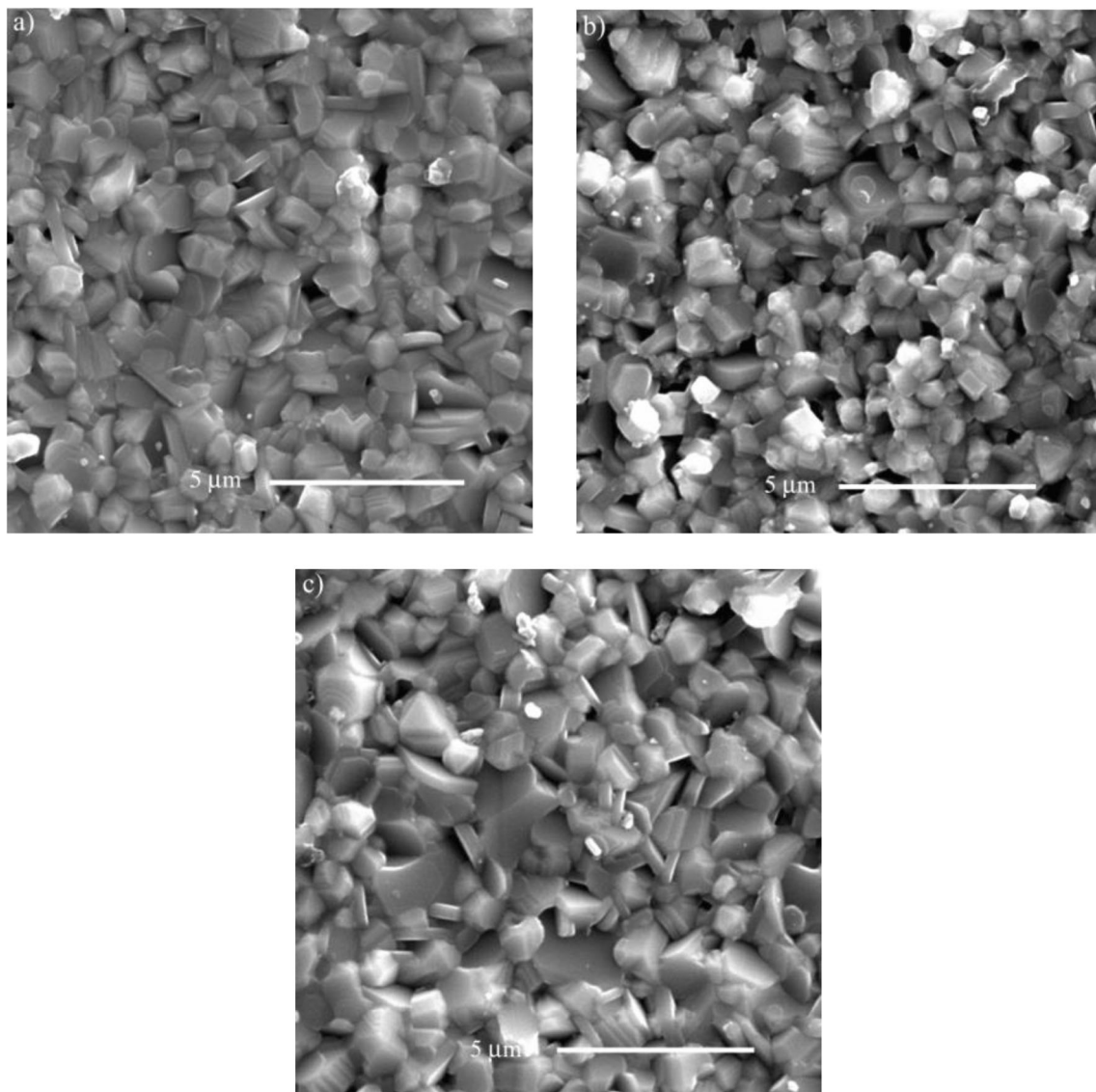


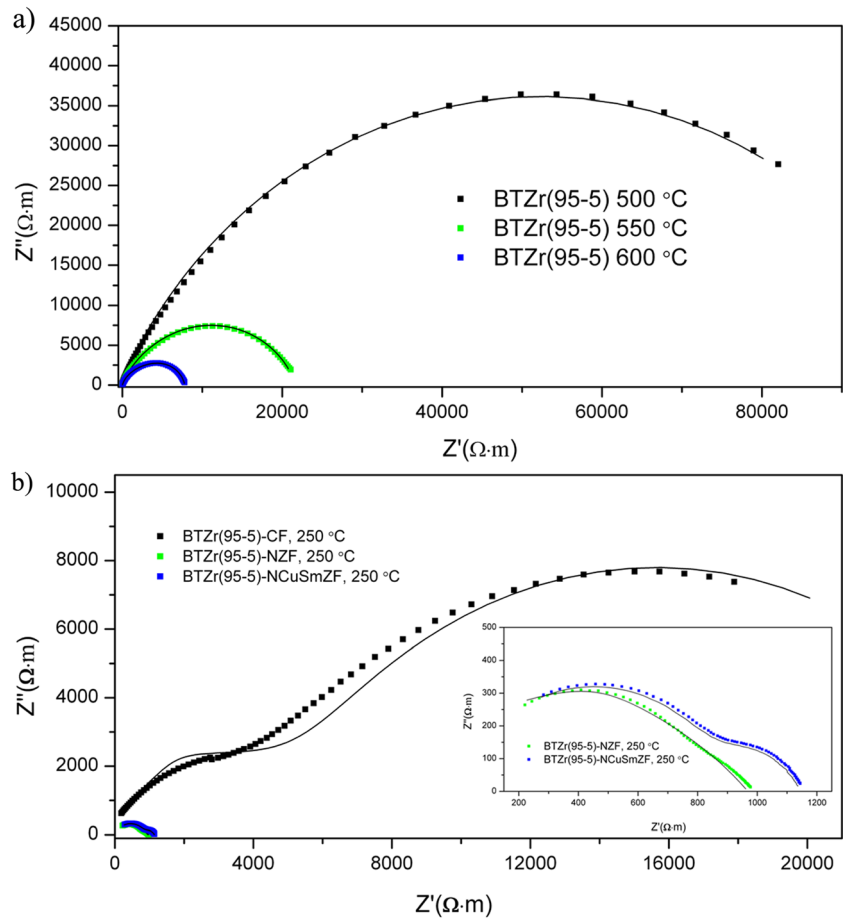
**Fig. 3** SEM images of: (a) BTZr(95–5)- NZF, (b) BTZr(95–5)- CF, (c) BTZr(95–5)- NCuSmZF ceramics

range for all composites. In the case of all samples the presence of two semicircular arcs are evident. Since, in composites materials the appearance of semicircular arcs can be attributed to the influence of different relaxation process such as grain and grain boundary or different crystallographic phases, it makes impedance analysis quite difficult. This electrical behavior can be represented in terms of three parallel R-CPE elements connected in series. Comparison of complex impedance plots with fitted data was analyzed using commercially available Z-view software. The best fit was achieved with three semicircular arc, one due to the influence of the grain boundary conduction at lower frequencies, the second due to the influence of grain conduction at higher frequencies and the third semicircular arc was observed corresponding to the influence of electrode. According to the different types of magnetic materials used for the MFs, temperature range of measurements differs. Due to that, it was not possible to compare

directly the resistivity of each sample at the same temperature. However, increasing of temperature led to grain and grain boundary resistivities decrease, indicating the semiconducting nature i.e. negative temperature coefficient of resistance. Impedance measurements for sample BTZr(95–5) were carried out in the temperature range far above Curie temperature, from 500 to 600 °C because of the very high resistivity of the material in large temperature region (shown at Fig. 4(a)). These curves show the phenomena of decentralization where the center of semicircle is centered below the real axis, making an angle with x-axis. The value of this angle is found to increase with temperature increase. The change of the total electrical resistivity with ferrite phase addition was expected. BTZr(95–5) has significantly higher resistivity compared to investigated composites due to the high conductivity of ferrites phase. Thus, in these composites the barium zirconium titanate mainly has the influence on the total



**Fig. 4** Impedance measurements for: (a) BTZr(95–5), (b) BTZr(95–5)-NZF, BTZr(95–5)-CF, BTZr(95–5)-NCuSmZF at different temperatures



resistivity, since the mass ratio between ferroelectric and ferrite phase in all three composites is 80–20. In composites, the highest resistivity was found for the BTZr(95–5)-CF (at the 250 °C) ceramics. In ferrites in the lower frequency region, where the influence of grain boundary conduction is dominant, hopping of the  $\text{Fe}^{2+}$  and  $\text{Fe}^{3+}$  is ineffective. With frequency increase, conductive grains become more active, resulting in increase of hopping process between  $\text{Fe}^{2+}$  and  $\text{Fe}^{3+}$  ions [31]. In both, composites and pure BTZr(95–5), besides above mention hopping motion in ferrites, the hopping of 3d electrons from  $\text{Ti}^{4+}$  to  $\text{Ti}^{3+}$  is also possible. Samples BTZr(95–5), BTZr(95–5)-NZF and BTZr(95–5)-NCuSmZF have  $R_g$  value which was higher in comparison with obtained value for  $R_{gb}$ , which suggested the grain contribution as a more influential effect in the total conduction of ceramics. Only in the case of BTZr(95–5)-CF the grain boundary effect can be ascribed as the dominant effect in total conduction. This sample has smaller grains in comparison with other investigated samples, which indicates the existence of a large number of grain boundaries.

The temperature dependence of the conductivity was given by equation:

$$\sigma = \sigma_0 \exp\left(-\frac{E_a}{k_b T}\right),$$

where  $\sigma_0$ ,  $E_a$ ,  $k_b$  represent preexponential factor, activation energy and Boltzmann constant, respectively, represented via Arrhenius plots (Fig. 5). The activation energy can be calculated from the slope of the given diagrams. The values of the grain and grain boundary activation energies were:  $E_{a,g} = 1.79$  eV,  $E_{a,gb} = 0.50$  eV for BTZr(95–5);  $E_{a,g} = 0.42$  eV,  $E_{a,gb} = 0.14$  eV for BTZr(95–5)-NZF;  $E_{a,g} = 0.81$  eV,  $E_{a,gb} = 1.01$  eV for BTZr(95–5)-CF and  $E_{a,g} = 0.54$  eV,  $E_{a,gb} = 0.39$  eV for BTZr(95–5)-NCuSmZF. Only for sample BTZr(95–5)-CF the activation energy for the conduction process through the grain boundaries has a higher value in the comparison with the grain. This indicates higher impact of grain boundaries on the total resistivity. Previous research has shown that the activation energy value above the 0.7 eV may correspond to the mobility of the defects in the crystal lattice of BT [32]. Explanation can be found also in defect chemistry. In the case when the activation energy reaches value of 1 eV, as reported in the literature, these values are attributed to the oxygen vacancies motion [33, 34]. The

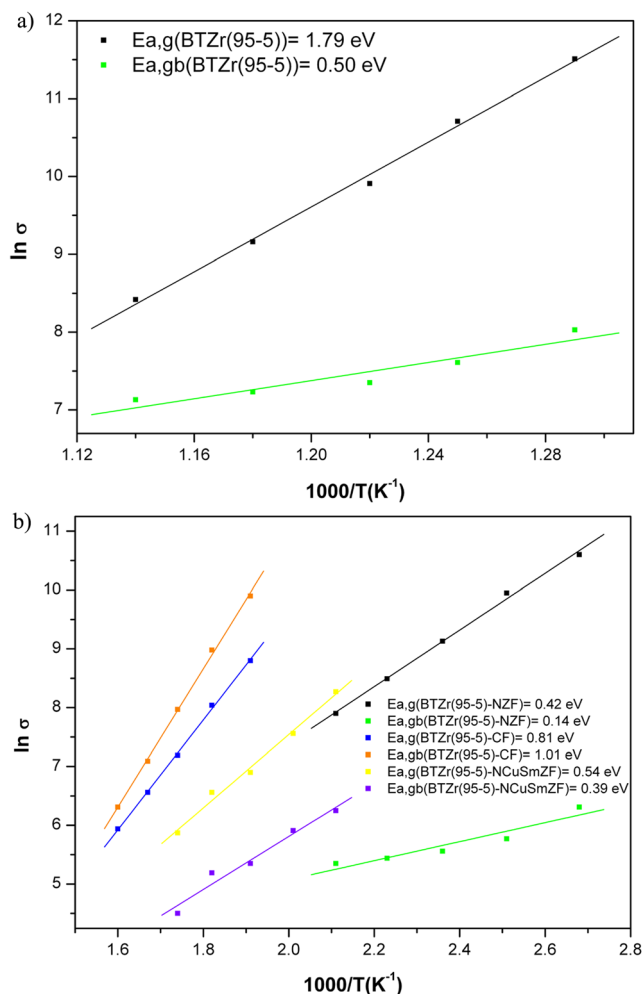


**Fig. 5** Arrhenius plots of grain and grain boundary conductivity for (a) BTZr(95–5), (b) BTZr(95–5)-NZF, BTZr(95–5)-CF, BTZr(95–5)-NCuSmZF

hopping of 3d electron among  $Fe^{2+}$  and  $Fe^{3+}$ ,  $Ni^{2+}$  and  $Ni^{3+}$  in ferrites as well as between  $Ti^{4+}$  and  $Ti^{3+}$  in barium zirconium titanate could play an important role in the conduction process as well. For other samples inverse trend was observed, where activation energy for grain has a higher value in the comparison with the grain boundary. It is probably due to smaller grains of BTZr(95–5)-CF in the comparison with other samples, as explained earlier in the text. Usually, activation energy for n-type polaronic conduction is less than 0.2 eV and above 0.2 eV for polaronic conduction of the holes. For pure BTZr(95–5) and all investigated composites, according to obtained values of  $E_a$  polaronic conduction of the holes can be considered. Also, the conduction at higher temperatures is suggested to be due to polaron hopping which is created possibly by the existence of the large effective mass and low mobility of the current carriers. For this type of conduction most important is the temperature dependent mobility of carries, rather than the temperature dependent concentration of carriers [35].

The variation of  $Z'$  with frequency at different temperatures for all ceramics is shown in Fig. 6. The value of  $Z'$  is higher in the low frequency range with a monotonous decrease with frequencies increase. Finally, in the high frequency region all the curves merge at 5 kHz for BTZr(95–5) and for all composites above 300 kHz. Decrease of the value of  $Z'$  with frequencies may be attributed to a slow dynamic relaxation process in all investigated samples due to space charge. At the higher frequencies merging all curves into single is connected with release of space charge [35, 36]. These materials exhibit a typical negative temperature coefficient of resistance (NTCR)-type behavior in semiconductors –since increase of the temperature led to a decrease of  $Z'$  magnitude. This increase in ac conduction can indicate the presence of defects like oxygen vacancies in the samples and originates mainly from the perovskite phase [37].

The variation of the imaginary part of impedance with frequency at different temperatures is shown in Fig. 7. The typical variation implied that  $Z''$  achieved a maximum value at the particular frequency, which is different for different temperatures. The nature of variation of  $Z''$  with frequency is characterized by a) the appearance of peaks at different frequency for BTZr(95–5) and investigated composites, b) a decrease in the height of the peaks toward to higher frequency side, c) the peaks were shifting towards higher frequencies with the temperature. There is an evident difference in curves shape for different ferromagnetic phase in the composites. Broadening of the peaks indicated the presence of phase dependent relaxation process in investigated composites. Also, this phenomenon is present in all samples with change in temperature, indicating the temperature dependent electrical relaxation in material. Possible explanation is the presence of immobile parts at the lower temperatures, and mobile defects, electrons and oxygen vacancies at higher temperatures [35, 38]. Heights of the peaks were found to decrease with the increase in frequency and temperature which point to the possible presence of charge polarization at the grain boundaries. For sample BTZr(95–5) they merge in the high frequency domain which indicate disappearance of charge polarization. Obviously, the same type of change occur also in the composites but at much higher frequencies. At higher temperatures, impedance is becoming more or less frequency independent. The addition of different ferrite phase affects the shapes of the curves differently. A similar shapes of the curves was obtained for BTZr(95–5) and BTZr(95–5)-CF and for BTZr(95–5)-NZF and BTZr(95–5)-NCuSmZF. First two samples show the lower frequency peaks correspond to the relaxation mechanism associated with grain boundaries and the other peaks are attributed to the grain contributions. Sample BTZr(95–5)-NCuSmZF also shows one less pronounced peak at lower frequencies. From this diagram grain boundary resistance and grain boundary capacitance can be calculated using the relationships  $C = 1 / 2\pi f_{max} R$ , where  $R = Z''_{max}$  (Table 1.).  $Z$

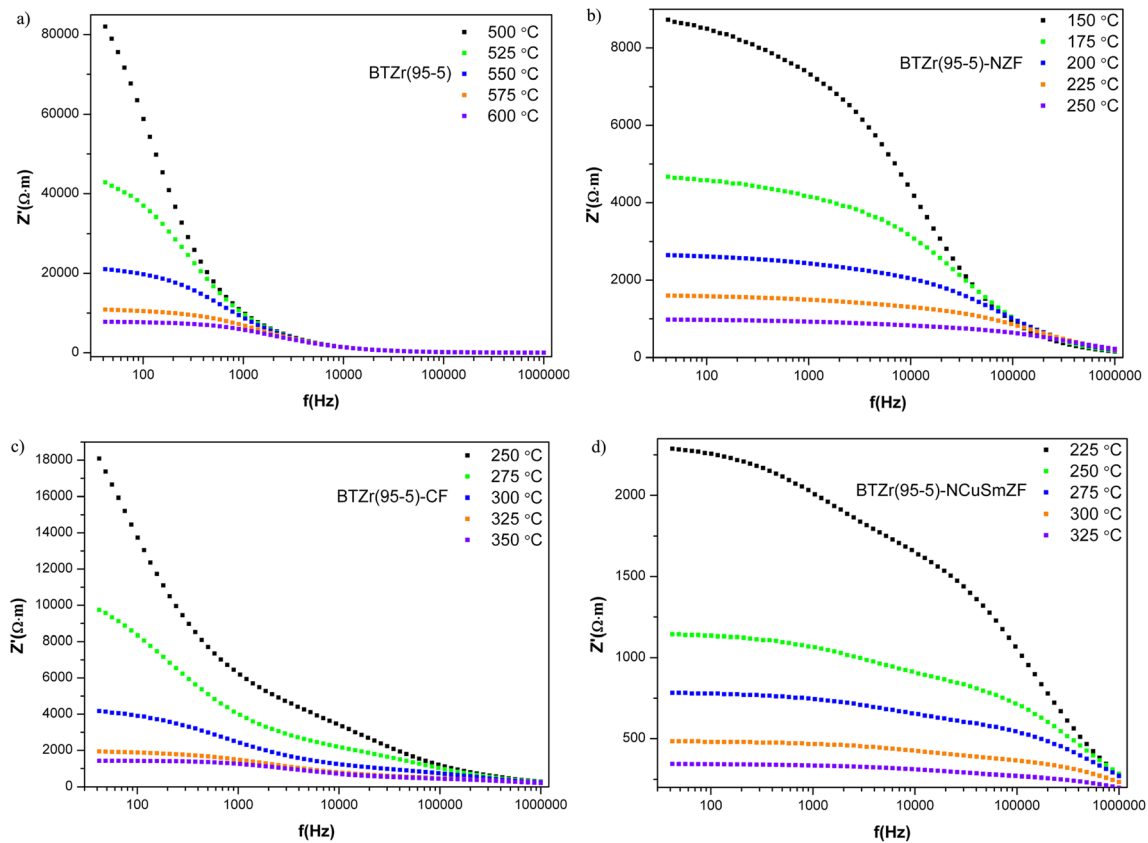


**Fig. 6** Variation of  $Z'$  with frequency at different temperatures for: (a) BTZr(95–5), (b) BTZr(95–5)-NZF, (c) BTZr(95–5)-CF and BTZr(95–5)-NCuSmZF ceramics

$f_{\max}$  is corresponding to maximum value of the  $Z''$  peak and  $f_{\max}$  is the associated frequency. Calculated values of capacitance for all investigated samples show that with the increase of temperature the value of capacitance decrease.

In order to confirmed the temperature dependence of dielectric relaxation normalized parameters  $Z''/Z_{\max}$  as a function of  $f/f_{\max}$  were analyzed for all investigated samples at different temperatures (Fig. 8.). In the BTZr(95–5) and BTZr(95–5)-NZF all data coincide into a single master curve at different temperatures. This can indicate that the contribution of relaxation time is temperature independent and all dynamical processes possess the same thermal energy under complex impedance formalism. Ceramics BTZr(95–5)-CF, curves overlap nicely in the lower frequency region, but at higher frequencies a second broad peak appears which point to temperature dependent relaxation time. Also, the appearance of these peaks is an indication of the transition from the long-range to a short range mobility [39]. On the other hand, samples that contain NCuSmZF, the temperature dependence was observed in whole frequency region. Two separate anomalies can be noticed and in comparison with CF, first anomaly appeared at much lower frequency.

Complex modulus plots,  $M''$ - $M'$ , at the different temperatures for BTZr(95–5) and composites are given in Fig. 9.

The complex electric modulus formalism can be used for separation of the electrode polarization effect from the grain boundary conduction process, to provide information about homogeneity of polycrystalline samples, to detect bulk properties such us conductivity relaxation times etc. [40, 41]. Values of  $M''$  and  $M'$  were calculated from following equations:  $M'' = \omega C_o Z_o$  and  $M' = \omega C_o Z''$ , respectively, where  $C_o$  is equal to  $\epsilon_o A/h$  and angular frequency  $\omega$  is equal to  $2\pi f$ . BTZr(95–5) showed two semi-circular arcs, which indicated the presence of two relaxation processes in this sample due to contribution of grain and grain boundary. For investigated composites, BTZr(95–5)-NZF, BTZr(95–5)-CF and BTZr(95–5)-NCuSmZF, one arc was observed indicating that the single relaxation process remained.

The frequencies dependence of variation of normalized parameters  $Z''/Z_{\max}$  and  $M''/M_{\max}$  for BTZr(95–5) at different temperatures are shown in Fig. 10 in order to determine if the conduction is localized or non-localized. In the case where  $Z''$  and  $M''$  peaks are separated in material exist localized relaxation otherwise when the peaks in these two curves are overlapping in material exist non-localized or a long range relaxations [42]. The mismatch between the peak frequency of the normalized  $M''$  and  $Z''$  which indicated the short-range



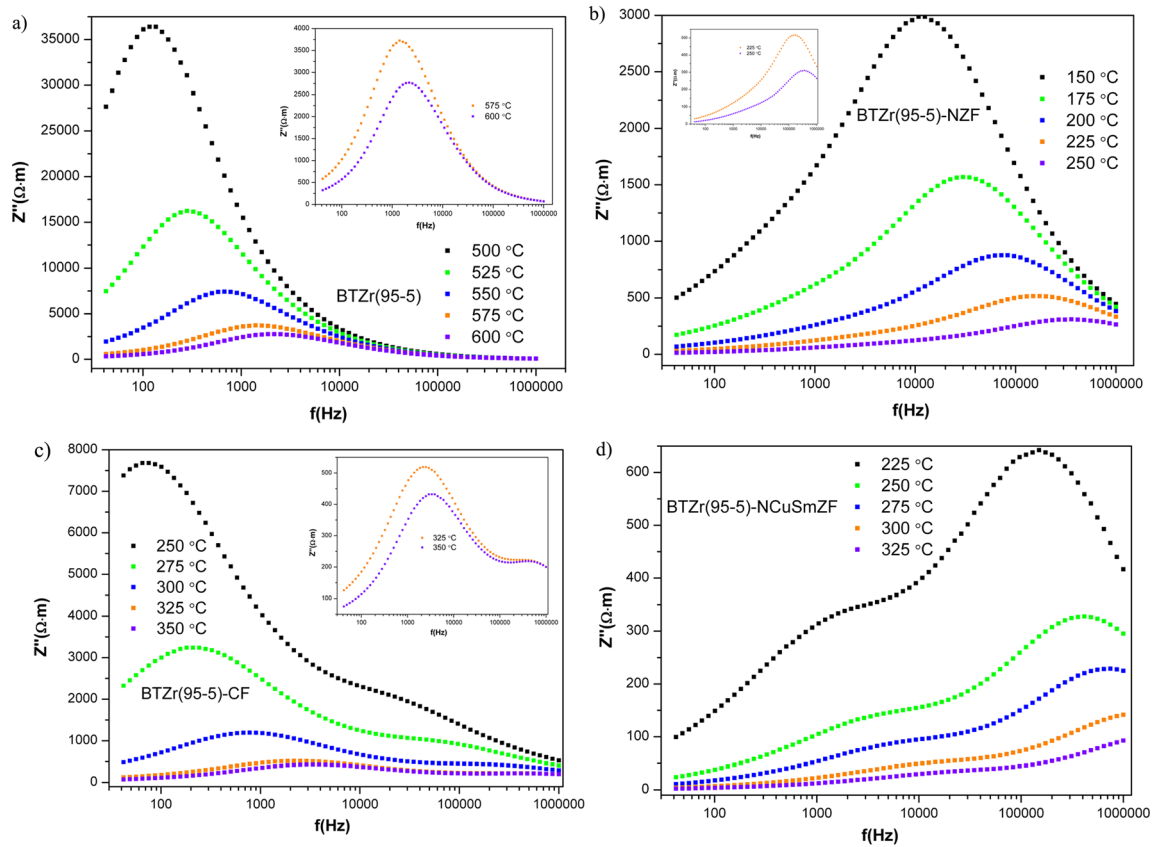


**Fig. 7** Imaginary parts of the impedance spectra as a function of frequency of (a) BTZr(95–5), (b) BTZr(95–5)-NZF, (c) BTZr(95–5)-CF, (d) BTZr(95–5)-NCuSmZF

conduction of localized charge carriers in material. This appearance indicated that polarization process is due to localized

conduction of multiple carriers which is in the accordance with results obtained from  $M''-f$  dependence.

**Table 1** Grain resistance, grain boundary resistance, total resistance and capacitance for investigated samples

Sample	T (°C)	from $Z''-Z'$			from $Z''-f$	
		$R_g(\Omega\cdot m)$	$R_{gb}(\Omega\cdot m)$	$R_{total}(\Omega\cdot m)$	$R_{gb}(\Omega\cdot m)$	$C_{gb}(nF/m)$
BTZr(95–5)	500	99,950	3070	103,020	72,870	17.62
	525	44,600	2020	46,620	32,472	17.61
	550	20,150	1550	21,700	14,838	16.26
	575	9550	1380	10,930	7428	15.16
	600	4550	1250	5800	5544	14.0
BTZr(95–5)-NZF	150	9210	260	9470	5986	2.34
	175	4880	230	5110	3142	1.73
	200	2700	210	2910	1754	1.26
	225	1550	120	1670	1036	1.00
	250	990	110	1100	620	0.71
BTZr(95–5)-CF	250	6630	19,850	26,480	15,312	137.4
	275	3110	7960	11,070	6496	119.6
	300	1330	2900	4230	2394	88.0
	325	710	1200	1910	1036	67.6
	350	380	550	930	866	54.9
BTZr(95–5)-NCuSmZF	225	1930	370	2300	1286	0.83
	250	990	210	1200	656	0.59
	275	710	180	890	456	0.54
	300	360	90	450	284	0.52
	325	190	52	250	160	0.49

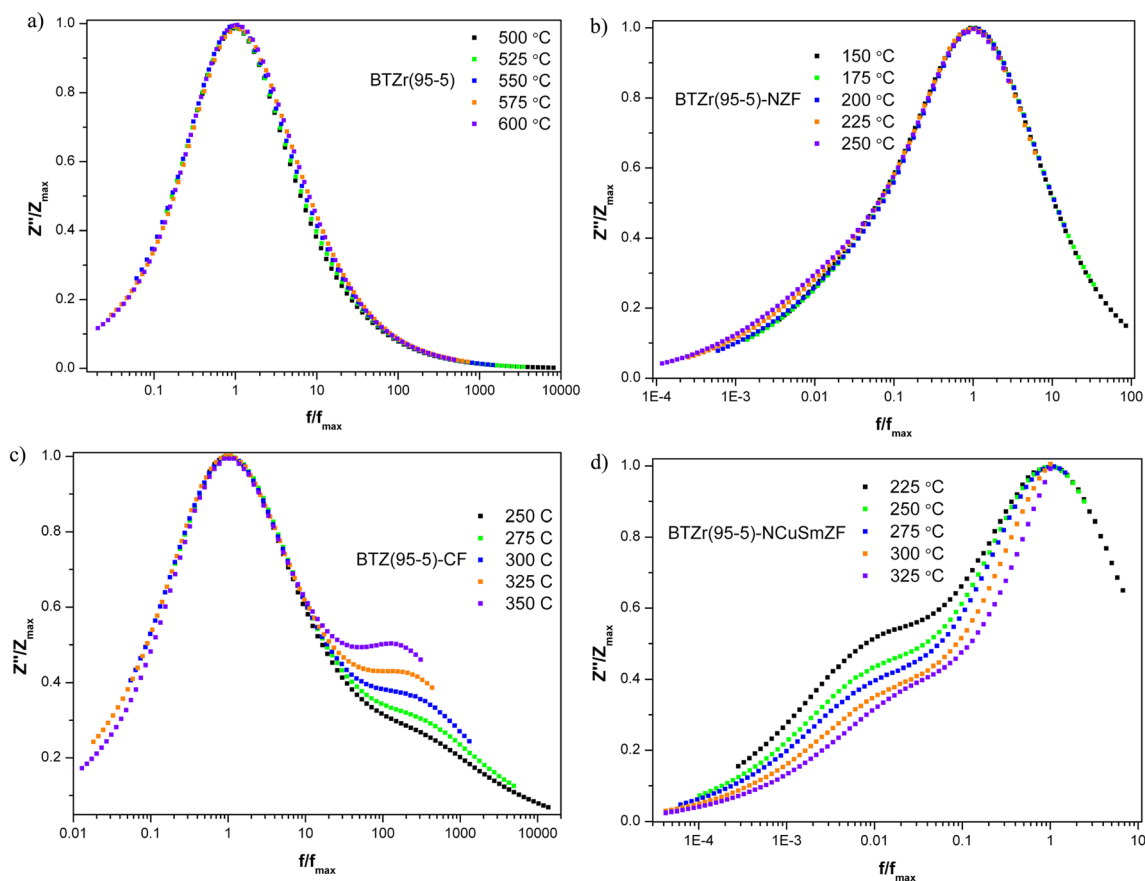


**Fig. 8** Frequency dependence  $Z''/Z_{\max}$  of (a) BTZr(95–5), (b) BTZr(95–5)-NZF, (c) BTZr(95–5)-CF, (d) BTZr(95–5)-NCuSmZF

### 3.3 AC and DC conductivity

AC conductivity,  $\sigma_{AC}$ , can be calculated from impedance measurements following the equation:

$$\sigma_{AC}(\omega) = \varepsilon_0 \varepsilon'' \omega$$

where  $\varepsilon_0$  is the permittivity of the free space, the  $\varepsilon''$  is imaginary part of dielectric permittivity and  $\omega$  is angular frequency. Figure 11. shows the logarithmic angular frequency dependence of AC conductivity at different temperatures. Two characteristic regions can be found, frequency independent region at the low frequencies which can be explained by the jump relaxation model and a dispersion region in the high frequency region. It can be suggested that, at low frequencies the conduction is probably through the hopping of charged particles from one localized state to another resulting in the long-range translation motion of charge carriers [43]. At high frequencies, AC conductivity has been found to obey a Jonscher power law which is expressed through the dependence:

$$\sigma(\omega) = \sigma(0) + A(T)\omega^n$$

where  $\sigma(\omega)$  is total conductivity,  $\sigma(0)$  is DC conductivity while  $A(T)$  and  $n$  are temperature and materials intrinsic

property dependent constant. The value of exponent  $n$  can be calculated from the slope of the presented plots and this value was used to explain conduction mechanism in the sample. Generally, value of  $n$  lies between 0 and 1 and here in the lower frequency region value of  $n$  is below 0.5 and can be attributed to the ionic hopping in the grains; in the high frequency region this value is between 0.5 and 1 and it can be attributed to the ionic hopping in the grain and grain boundary regions [10, 43].

### 3.4 Ferroelectric properties

The results of polarization vs. electric field measurements have shown the influence of magnetic phases type and concentration on the ferroelectric properties of the composites (Fig. 12. and Table 2.). These ferroelectric loops were obtained by applying the electrical field in the range of 10–38 kV/cm depending on different breakdown field for investigated ceramic samples. Due to high conductivity of ferrite phases and presence of interfacial polarization, the shapes of these curves differed from the conventional ferroelectric materials [2]. Because of presence of non-saturated ferroelectric loops it is not possible to talk about remnant or saturation polarization and coercive field. The following are comparison for these

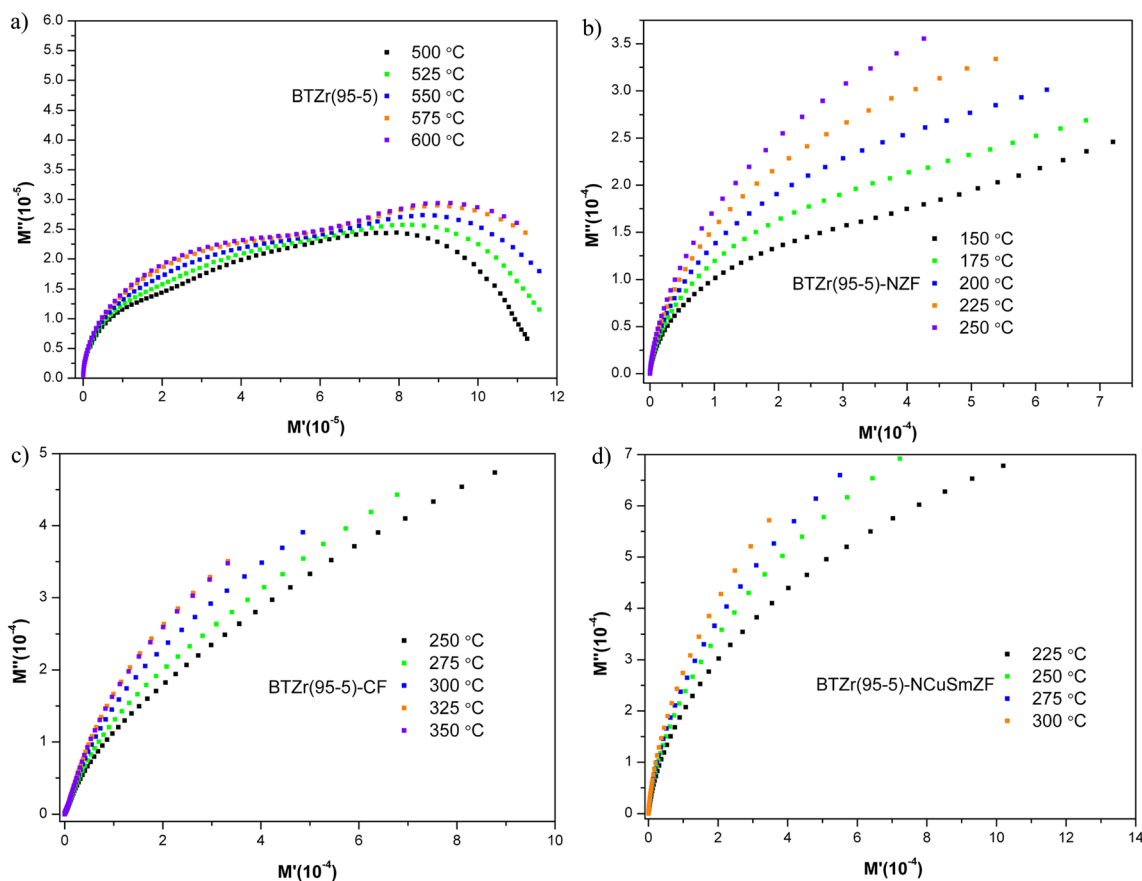


**Fig. 9** Complex electric modulus plane plot of (a) BTZr(95–5), (b) BTZr(95–5)-NZF, (c) BTZr(95–5)-CF, (d) BTZr(95–5)-NCuSmZF

values for different samples at certain field strength. The values of remnant polarization at the 20 kV/cm were: 0.50, 2.55, 0.31, 2.94  $\mu\text{C}/\text{cm}^2$  for the composites BTZr(95–5), BTZr(95–5)-NZF, BTZr(95–5)-CF, BTZr(95–5)-NCuSmZF, respectively and for the saturation polarization were 1.29, 2.89, 0.48 and 3.89  $\mu\text{C}/\text{cm}^2$ . Some of the samples also handle higher field strength. However, due to the existence of non-saturated ferroelectric loops, the comparison of  $P_r$  and  $P_s$  was

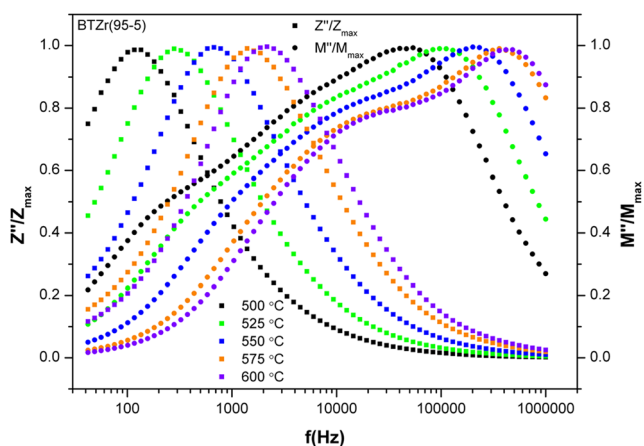


**Fig. 10**  $Z''/Z_{\text{max}}$  and  $M''/M_{\text{max}}$  as a function of frequency for: BTZr(95–5) at different temperatures

done at the appropriate field strength. Compared with the literature data, the value of  $P_r$  and  $E_c$  for BTZr(95–5) is lower in comparison with BTZr(95–5) obtained with solid state reaction method [18]. The reason for this is in the fact that BTZr(95–5) obtained with solid state reaction has better density (5800  $\text{g}/\text{cm}^3$  recalculated 95.8% of theoretical) in comparison with BTZr(95–5) obtained with auto-combustion reaction (86.0% of theoretical value). At 20 kV BTZr(95–5) has higher values of  $P_r$  and  $P_s$  in comparison with BTZr(95–5)-CF but lower value of  $P_r$  and  $P_s$  in comparison with BTZr(95–5)-NZF and BTZr(95–5)-NCuSmZF. BTZr(95–5) was sintered at 1200 °C which is lower temperature in comparison with sintering temperature for composites (1300 °C). Sample with higher temperature of sintering usually possesses better density and better electrical properties. The experience from previous studies on similar compositions, BTZr(95–5) would have been better electrical properties at 1300 °C, but this sample could not be sintered at higher temperature due to secondary phase formation [44, 45]. Also, smaller grains of investigated sample affect the poor ferroelectric properties. There are many data in literature for the influence of density and the grain size on ferroelectric properties of the ceramics. Y. Tan et al. claimed that increase in grain size led to decrease in  $E_c$  [46]. This is one of the reasons why BTZr(95–5) – NZF have

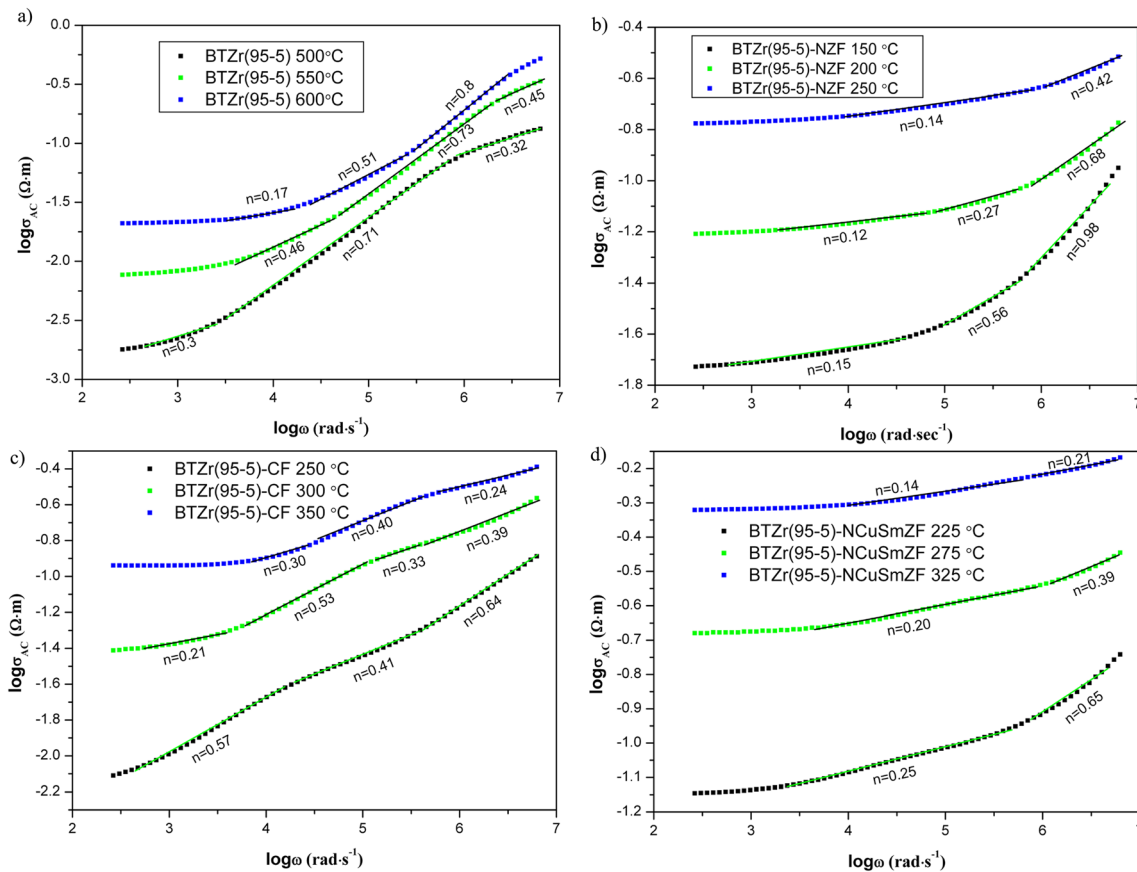


**Fig. 11** Angular frequency dependence ac conductivity of: (a) BTZr(95–5), (b) BTZr(95–5)-NZF, (c) BTZr(95–5)-CF, (d) BTZr(95–5)-NCuSmZF at different temperatures

higher value of  $E_c$  in comparison with BTZr(95–5)-CF and BTZr(95–5)-NCuSmZF. Another reason for the highest value of coercive field for BTZr(95–5)-NZF can be probably the presence of large number of oxygen vacancies which inhibits the movement of domains causing domain wall pinning [47, 48]. These oxygen vacancies may originate from sintering in air where the oxygen loss during the sintering can produce oxygen vacancies as well as free electrons. Also,  $\text{Ti}^{4+}$  is chemically less stable and it easily change to  $\text{Ti}^{3+}$ , thus the formation of oxygen vacancies occur in these kind of materials. Expectedly, composites possess higher value of  $E_c$  in comparison with BTZr(95–5) because the composites are more difficult to be polarized due to ferrite phase which can act as a obstacle for the movement of the domains. On the other hand, the increase of the grain size of investigated composites can lead to the increase of value of  $P_r$  and  $P_s$ . The increase of grain size can enhance the domain switching ability and enable the improvement of the ferroelectric properties,  $P_r$  and  $P_s$ . Also, high number of grain boundaries in the ceramics with small grains can result with decrease of  $P_r$  and  $P_s$ , since the grain boundaries possess low permittivity and poor ferroelectricity and can affect greatly the reduction of polarization [15, 49]. It is difficult to say which ferrite phase has the greatest impact on ferroelectric properties because none of the material

did not reach the saturation. The highest value of  $P_r$  and  $P_s$  possesses BTZr(95–5)-NCuSmZF which recommend this material as potentially more applicable for ferroelectric application.

### 3.5 Leakage current density

In order to study conductivity mechanism of the BTZr(95–5) and BTZr(95–5)-NZF, BTZr(95–5)-CF, BTZr(95–5)-NCuSmZF, the leakage current density ( $j$ ) was measured at room temperature as a function of static electric field ( $E$ ). These dependences are presented on the semi-log and log-log plots (Fig. 13.) and the slope of the curve in logarithmic plot determine the nature of conduction. For all samples, two regions of different slopes were observed. In that way, mechanism of the conduction present in these materials was predicted as follows: grain boundary limited conduction (GBLC), ohmic conduction mechanism, space charge limited conduction (SCLC) or trap-controlled SCLC mechanism [50, 51]. For the BTZr(95–5) sample, at the high field region, the value of  $n$  larger than 2 suggest the presence of trap controlled SCLC conduction mechanism. In low field region, slope was found to be less than 1 which suggested the existence of grain boundary limited conduction.

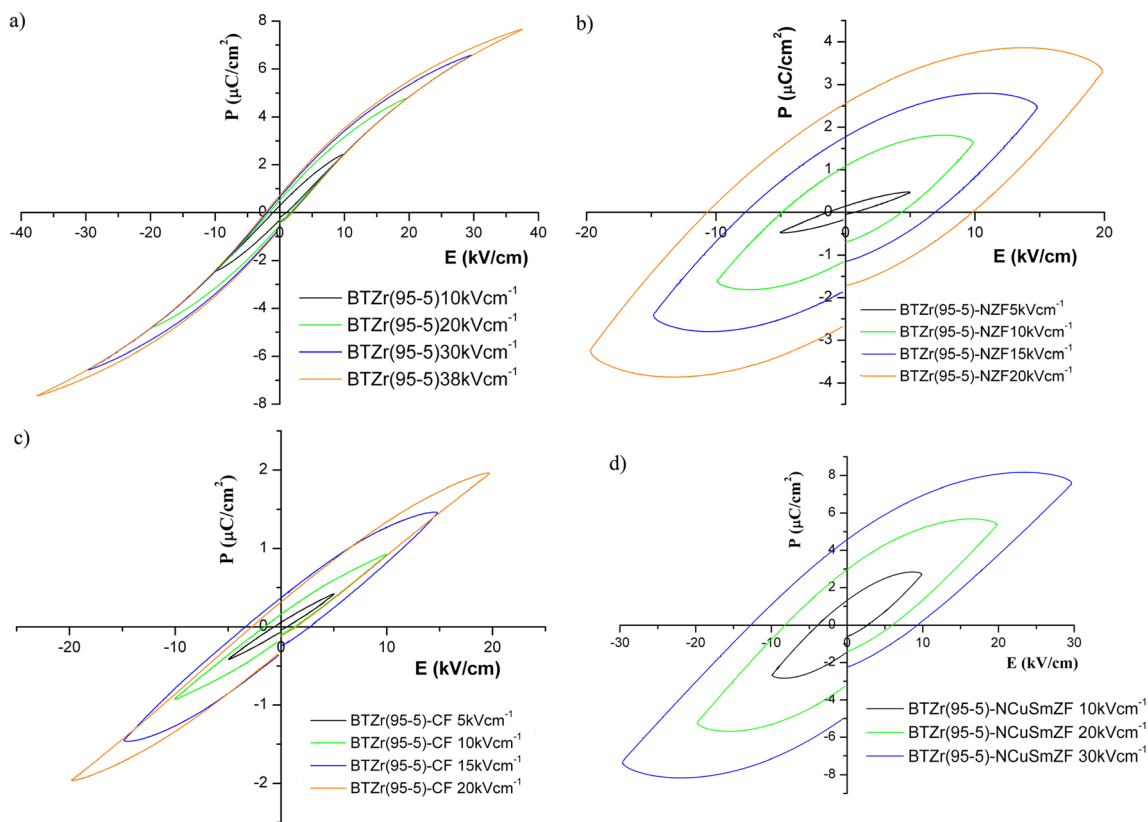


**Fig. 12** Hysteresis P-E loops for (a) BTZr(95–5), (b) BTZr(95–5)-NZF, (c) BTZr(95–5)-CF, (d) BTZr(95–5)-NCuSmZF

For investigated composites samples it was observed that the highest value of leakage current density possessed BTZr(95–5)-NCuSmZF and the lowest for BTZr(95–5)-CF in the whole electric field region. Indeed, the BTZr(95–5)-CF showed higher resistivity than BTZr(95–5)-NZF and BTZr(95–5)-NCuSmZF. This also can indicate also the presence of free charge carriers (oxygen vacancies in this case) in BTZr(95–5)-CF, formed due to Fe<sup>3+</sup> reduction to Fe<sup>2+</sup>, which is possibly not so dominant in two other samples [52]. Samples BTZr(95–5)-CF and BTZr(95–5)-NZF in low field region the value of *n* is between 1 and 1.5 which suggested the existence of ohmic conduction mechanism and in high field region this value is between 1.5 and 2 which pointed on the existence of space charge limited conduction. In the region with ohmic conduction mechanism the thermally generated free carriers density is higher than the density of injected charge carriers while in the region with space charge limited conduction the injected charge carriers dominate the conduction. BTZr(95–5)-NCuSmZF showed the same behavior in low field region, but in the higher field region the value of *n* is higher than 2 which is characteristic of trap controlled SCLC mechanism.

### 4 Conclusions

The multiferroic composites of barium zirconium titanate-ferrites (NZF, CF, NCuSmZF) were obtained by mixing of

previously prepared powders by auto-combustion synthesis. XRD confirmed the presence of pure phase of barium zirconium titanate and ferrites phases. From SEM analysis can be noticed that the average grain sizes are under 0.8 nm for

**Table 2** Saturation polarization, remnant polarization and coercive field for measured samples

Sample	kV/cm	P <sub>s</sub> (μC/cm <sup>2</sup> )	P <sub>r</sub> (μC/cm <sup>2</sup> )	E <sub>c</sub> (kV/cm)
BTZr(95–5)	10	0.7208	0.2958	1.076
	20	1.288	0.5049	1.614
	30	1.774	0.6454	1.973
	38	2.225	0.7574	2.188
BTZr(95–5)-NZF	5	0.2035	0.1398	0.6609
	10	1.232	1.080	4.362
	15	2.046	1.781	6.958
	20	2.889	2.552	9.939
BTZr(95–5)-CF	5	0.0949	0.0534	0.902
	10	0.2416	0.1567	1.210
	15	0.4464	0.2616	2.681
	20	0.4832	0.3134	3.549
BTZr(95–5)-NCuSmZF	10	1.651	1.308	2.652
	20	3.888	2.937	5.981
	30	5.879	4.597	9.398



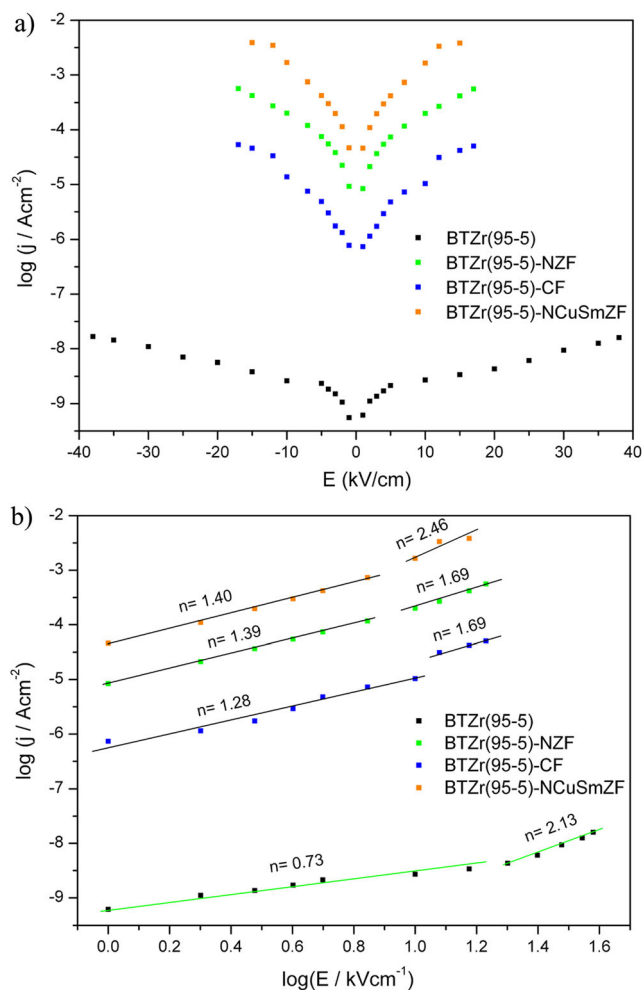


**Fig. 13** Leakage measurements: (a)  $\log E$ - $j$ , (b)  $\log E$ - $\log E$ , for BTZr(95–5), BTZr(95–5)-NZF, BTZr(95–5)-CF, BTZr(95–5)-NCuSmZF

obtained composites with two different types of grains. Impedance analysis has shown the presence of phase dependent relaxation process in all investigated composites and the temperature dependent electrical relaxation in material. The value of calculated energy activation indicated the presence of polaronic conduction of the holes type. Investigation of AC and DC conductivity confirmed the presence of conduction mechanism based on hopping of charged particles from one localized state to another at low frequencies and for the higher frequencies AC conductivity have been found to obey a Jonscher power law. P-E hysteresis loops have shown that ferroelectric properties of obtained composites are being reduced in comparison with pure BZrT(95–5) because of existence of non ferroelectric ferrite phase. The analysis of the dependence of the leakage-current density on the applied electrical field showed that all, pure BTZr(95–5) and composites have four different regions of conduction: region with grain boundary limited conduction (GBLC), region with ohmic conduction mechanism, region with space charge limited conduction (SCLC) and region with trap-controlled SCLC mechanism.

Based on presented research of composites it can be pointed that BZrT(95–5)-CF showed better electrical properties, microstructure homogeneity and density compared to other investigated composites. Also, this sample possesses the lowest leakage current and the highest resistivity among the investigated composites. Future research will be focused on the investigation of the magnetic properties as well as the application of this material based on its piezoelectric and magnetoelectric characteristics.

**Acknowledgments** The authors gratefully acknowledge the financial support of the ministry of Education, Science and Technological Development of the Republic of Serbia (Project III45021).

## References

1. H. Schmid, *Ferroelectric* **132**, 317 (1994)
2. W. Eerenstein, N. Mathur, J. Scott, *Nature* **442**(7104), 759–765 (2006)
3. W. Prellier, M. Singh, P. Murugavel, *J. Phys. Condens. Matter.* **17**(30), R803–R832 (2005)
4. R. Mondal, B. Murty, V. Murthy, *Mater. Chem. Phys.* **167**, 338–346 (2015)
5. T. Kimura, T. Goto, H. Shintani, K. Ishizaka, T. Arima, Y. Tokura, *Nature* **426**(6962), 55–58 (2003)
6. A. Dzunuzovic, M. Vijatovic Petrovic, B. Stojadinovic, N. Ilic, J. Bobic, C. Foschini, M. Zaghet, B. Stojanovic, *Ceram. Int.* **41**(10), 13189–13200 (2015)
7. R. Pandya, U. Joshi, O. Caltun, *Procedia Mater. Sci.* **10**, 168–175 (2015)
8. M. Bernardo, T. Jardiel, M. Peiteado, A. Caballero, M. Villegas, *J. Eur. Ceram. Soc.* **31**(16), 3047–3053 (2011)
9. T. Karthik, A. Srinivas, V. Kamaraj, V. Chandrasekeran, *Ceram. Int.* **38**(2), 1093–1098 (2012)
10. M. Vijatovic Petrovic, R. Grigalaitis, A. Dzunuzovic, J. Bobic, B. Stojanovic, R. Salasevicius, J. Banys, *J. Alloy. Compd.* **749**, 1043–1053 (2018)
11. A. Dzunuzovic, M. Vijatovic Petrovic, J. Bobic, N. Ilic, M. Ivanov, R. Grigalaitis, J. Banys, B. Stojanovic, *Ceram. Int.* **44**(1), 683–694 (2018)
12. J. Bobić, M. Ivanov, N. Ilić, A. Dzunuzović, M. Vijatović Petrović, J. Banys, A. Ribic, Z. Despotovic, B. Stojanovic, *Ceram. Int.* **44**(6), 6551–6557 (2018)
13. L. Mitoseriu, *Bol. Soc. Esp. Ceram.* **44**(3), 177–184 (2005)
14. N. Adhlakha, K. Yadav, *Smart Mater. Struct.* **21**(11), 115021 (2012)
15. M. Vijatovic Petrovic, A. Radojkovic, J. Bobic, A. Dzunuzovic, N. Ilic, B. Stojanovic, *J. Mater. Sci.* **54**(8), 6038–6052 (2019)
16. M. Vijatovic Petrovic, J. Bobic, in *Magnetic, ferroelectric, and multiferroic metal oxides*, ed. by B. D. Stojanovic. (Elsevier Publisher, Amsterdam, 2018), pp. 35–49
17. N. Binhayeeniyi, P. Sukvisut, C. Thanachayanont, S. Muensit, *Mater. Lett.* **64**(3), 305–308 (2010)
18. Z. Yu, C. Ang, R. Guo, A. Bhalla, *J. Appl. Phys.* **92**(3), 1489–1493 (2002)
19. F. Moura, A. Simoes, B. Stojanovic, M. Zaghet, E. Longo, J. Varela, *J. Alloy. Compd.* **462**(1–2), 129–134 (2008)
20. C. Nan, M. Bichurin, S. Dong, D. Viehland, G. Srinivasan, *J. Appl. Phys.* **103**(3), 031101 (2008)

21. N. Hosni, K. Zehani, T. Bartoli, L. Bessais, H. Maghraoui-Meherzi, *J. Alloy. Compd.* **694**, 1295–1301 (2017)
22. M. Niyaiifar, H. Shalilian, A. Hasanpour, Proceedings of the 4<sup>th</sup> International Conference on Nanostructures (ICNS4) 12–14 March, 2012, Kish Island, I.R. Iran
23. V. Jancarik, M. Soka, M. Usakova, R. Dosoudil, *J. Electr. Eng.* **66**, 116 (2015)
24. M. Soka, J. Slama, A. Gruskova, R. Dosoudil, V. Jancarik, J. Franek, *IEEE T. Magn.* **48**(4), 1573–1576 (2012)
25. B. Suryanarayana, K. Chandra Mouli, V. Raghavendra, B.B. Parvateesam, National Conference on Advanced Functional Materials and Computer Applications in Materials Technology (CAMCAT-2014)
26. L. Gama, A. Diniz, A. Costa, S. Rezende, A. Azevedo, D. Comejo, *Physica B* **384**(1–2), 97–99 (2006)
27. A. Sattar, A. Samy, *J. Mater. Sci.* **37**(20), 4499–4502 (2002)
28. A. Dzunuzovic, M. Vijatovic Petrovic, N. Ilic, J. Bobic, B. Stojanovic, *Process Appl. Ceram.* **13**, 113 (2019)
29. R. Sagar, R. Raibagkar, *J. Alloy. Compd.* **549**, 206–212 (2013)
30. A. Mahmood, A. Naeem, Y. Iqbal, *Ceram. Int.* **42**(4), 4860–4865 (2016)
31. R. Qindeel, N. Alonizan, *Curr. Appl. Phys.* **18**(5), 519–525 (2018)
32. C. Ciomaga, A. Neagu, M. Pop, M. Airimioaei, S. Tascu, G. Schileo, C. Galassi, L. Mitoseriu, *J. Appl. Phys.* **113**, 074103 (2013)
33. J. Irvine, D. Sinclair, A. West, *Adv. Mater.* **2**(3), 132–138 (1990)
34. G. Yang, E. Dickey, C. Randall, D. Barber, P. Pinceloup, M. Henderson, R. Hill, J. Beeson, D. Skamser, *J. Appl. Phys.* **96**(12), 7492–7499 (2004)
35. K. Verma, S. Sharma, *Phys. Status Solidi B* **249**(1), 209–216 (2012)
36. O. Reymond, R. Font, N. Almodovac, J. Poetelles, J. Siqueiros, *J. Appl. Phys.* **97**(8), 084107 (2005)
37. M.A. Rafiq, M.N. Rafiq, K. Saravanan, *Ceram. Int.* **41**(9), 11436–11444 (2015)
38. T. Badapanda, S. Sarangi, B. Behera, S. Anwar, *Curr. Appl. Phys.* **14**(9), 1192–1200 (2014)
39. P. Kumar, S. Singh, M. Spah, J. Juneja, C. Prekash, K. Raina, *J. Alloys Compd.* **489**(1), 59–63 (2010)
40. S. Sen, S.K. Mishra, S.K. Das, A. Tarafdar, *J. Alloys Compd.* **453**(1–2), 395–400 (2008)
41. M. Dar, V. Verma, S. Gairola, W. Siddiqui, R. Singh, R. Kotnala, *Appl. Surf. Sci.* **258**(14), 5342–5347 (2012)
42. R. Gerhardt, *J. Phys. Chem. Solids* **55**(12), 1491 (1994)
43. S. Kumar, K. Varma, *Curr. Appl. Phys.* **11**(2), 203–210 (2011)
44. M. Vijatovic Petrovic, J. Bobic, H. Ursic, J. Banys, B. Stojanovic, *J. Sol-Gel Sci. Technol.* **67**(2), 267–272 (2013)
45. M. Vijatovic Petrovic, J. Bobic, R. Grigalaitis, N. Ilic, A. Dzunuzovic, V. Jankauskaite, J. Banys, B. Stojanovic, *Ceram. Int.* **41**(9), 11365–11371 (2015)
46. Y. Tan, J. Zhang, Z. Wu, C. Wang, V. Koval, B. Shi, H. Ye, R. McKinnon, G. Viola, H. Yan, *Sci. Rep.* **5**(1), 9953 (2015)
47. P. Pahuja, R. Kontala, R. Tandol, *J. Alloy. Compd.* **617**, 140–148 (2014)
48. N. Kitamura, T. Mizoguchi, T. Itoh, Y. Idemoto, *J. Solid State Chem.* **210**, 279 (2014)
49. N. Buatip, N. Promsawat, N. Pisitpipathsin, O. Namsar, P. Pawasri, K. Ounsung, K. Phabsimma, S. Rattanachan, P. Janphuang, S. Projprapai, *Integr. Ferroelectr.* **187**(1), 45–52 (2018)
50. H. Du, W. Liang, Y. Li, M. Gao, Y. Zhang, C. Chen, Y. Lin, *J. Alloy. Compd.* **645**, 166 (2015)
51. V. Janardhanam, Y. Park, K. Ahn, C. Choi, *J. Alloy. Compd.* **534**, 37–41 (2012)
52. S. Godara, B. Kumar, *Ceram. Int.* **41**(5), 6912–6919 (2015)

**Publisher's note** Springer Nature remains neutral with regard to jurisdictional claims in published maps and institutional affiliations.